INTERNATIONAL JOURNAL FOR NUMERICAL METHODS IN FLUIDS
Int. J. Numer. Meth. Fluids 2007; **54**:269–294
Published online 30 November 2006 in Wiley InterScience (www.interscience.wiley.com). DOI: 10.1002/fld.1395

Three-dimensional instability of axisymmetric flows: Solution of benchmark problems by a low-order finite volume method

Alexander Y. Gelfgat*, †

School of Mechanical Engineering, Faculty of Engineering, Tel-Aviv University, Ramat Aviv 69978, Israel

SUMMARY

Several problems on three-dimensional instability of axisymmetric steady flows driven by convection or rotation or both are studied by a second-order finite volume method combined with the Fourier decomposition in the periodic azimuthal direction. The study is focused on the convergence of the critical parameters with mesh refinement. The calculations are done on the uniform and stretched grids with variation of the stretching. Converged results are reported for all the problems considered and are compared with the previously published data. Some of the calculated critical parameters are reported for the first time. The convergence studies show that the three-dimensional instability of axisymmetric flows can be computed with a good accuracy only on fine enough grids having about 100 nodes in the shortest spatial direction. It is argued that a combination of fine uniform grids with the Richardson extrapolation can be a good replacement for a grid stretching. It is shown once more that the sparseness of the Jacobian matrices produced by the finite volume method allows one to enhance performance of the Newton and Arnoldi iteration procedures by combining them with a direct sparse linear solver instead of using the Krylov-subspace-based iteration methods. Copyright © 2006 John Wiley & Sons, Ltd.

Received 27 July 2006; Revised 1 October 2006; Accepted 2 October 2006

KEY WORDS: finite volume methods; hydrodynamic stability; Newton iteration; Arnoldi iteration

1. INTRODUCTION

In a recent paper [1], the convergence of the critical parameters corresponding to instabilities of convective flows in rectangular cavities was studied. It was shown that using a low-order numerical method the acceptable accuracy of the calculated critical parameters can be reached only on grids consisting of 100^2 nodes or more. The necessity to use a low-order method is dictated by many practical problems, for which application of higher-order methods is too complicated. Such practical

*Correspondence to: Alexander Y. Gelfgat, School of Mechanical Engineering, Faculty of Engineering, Tel-Aviv University, Ramat Aviv 69978, Israel.
†E-mail: gelfgat@eng.tau.ac.il

Contract/grant sponsor: Israel Science Foundation; contract/grant number: 156/05

problems, among which we can mention the problem of stability of melt flow in bulk crystal growth processes, usually have an axisymmetric geometry, so that an unperturbed flow is also expected to be axisymmetric and steady. It is well known that with the increase of a forcing parameter, e.g. Reynolds, Grashof, Marangoni number, these flows become unstable and transform into an axisymmetric oscillatory or into three-dimensional steady or oscillatory state. In the latter case, the axisymmetry of the initial base state is broken and three-dimensional calculations are needed to model supercritical flows.

Due to existing computer restrictions, fully three-dimensional unsteady computations usually cannot be done on fine grids. Performing calculations using coarse grids without a detailed convergence study can lead to qualitatively wrong results. The corresponding examples are given below. This accuracy problem can be partially removed for the axisymmetric base flows if the study is restricted to their linear stability with respect to all possible infinitesimal perturbations. When the flow region is axisymmetric, the flow can be looked for as a Fourier series, with the Fourier decomposition applied in the periodic azimuthal direction. In a fully non-linear case, the Fourier modes interact, so that the Fourier decomposition does not yield a significant reduction in the number of degrees of freedom corresponding to a chosen numerical model. However, when linear stability of an axisymmetric base flow is considered, the problem for each Fourier mode separates from the others. This allows one to replace a fully three-dimensional problem by a series of two-dimensional-like computations, so that every computation treats a significantly smaller amount of degrees of freedom. In this way rather fine grids can be used. In the following calculations, we use the grids consisting of up to 500^2 nodes in the meridional plane.

In this paper, we use a low-order finite volume method to study the axisymmetry-breaking three-dimensional instabilities of axisymmetric steady base flows. We consider several benchmark problems and focus our attention on the convergence of the critical parameters with the grid refinement and on the effect of grid stretching. It should be mentioned that the benchmark problems for axisymmetric flows, especially including their three-dimensional instability, are not established as well as the benchmark problems in rectangular cavities considered in [1]. We can mention recently formulated benchmark [2] and results of [3–6], which were used for the benchmarking purposes in [7–14] and other studies. Also, the spectral and pseudospectral methods that yield a high-accuracy benchmark data for the flows in rectangular enclosures are not so usual for the cylindrical domains. The spectral, pseudospectral and collocation methods were successfully applied in [3–6, 10, 11], while in other studies [12–18] the authors preferred to use lower-order finite volume or finite element methods. For more complicated problems directly related to simulation of flows in different technological processes (e.g. [7, 8]), the low-order methods seem to be the only possible choice. This indicates once more on the necessity to study the convergence of the critical parameters calculated by a low-order numerical approach. Note also that most of flows considered below have discontinuities in boundary conditions. Such discontinuities are rather common for both model flows and more complicated technological applications. A special care should be taken to treat a discontinuity by a spectral method [5, 6, 9], and even then the discontinuity can cause undesirable numerical problems when three-dimensional perturbations are calculated [9]. For low-order methods, such discontinuities do not pose any technical difficulties, however can slow down the convergence.

In the following, we consider several model axisymmetric flows in cylindrical enclosures starting from the natural convection flow in a non-uniformly heated cylinder. Then we consider two different flows driven by the thermocapillary convection and a swirling isothermal flow driven by rotation of one of boundaries. Finally, we consider a model flow driven by both natural convection and rotation.

DOI: 10.1002/fld

Along with the grid refinement and stretching, we study the possibility to improve numerical results by the Richardson extrapolation.

The numerical procedure used here for calculation of the axisymmetric steady states and study of their stability is similar to one used in [1]. The governing equations are discretized using the finite volume method in radial and axial directions and by applying the Fourier decomposition in the azimuthal direction. Steady states are calculated by the exact Newton iteration with fully calculated Jacobian matrix. The eigenproblem needed for the stability analysis is solved by the Arnoldi method using the ARPACK package[‡] [19]. As in [1], the computations are made effective with the help of MUMPS multifrontal direct solver,[§] which is used for the calculation of the LU decomposition of the sparse Jacobian matrices.

Performing the convergence studies up to grids of 500^2 nodes we show that similar to the flows in rectangular cavities one needs about 100 grid points in the shortest spatial direction to obtain reliable results on the axisymmetry breaking of axisymmetric flows. We show that the grid stretching can significantly improve the results, but not every stretching is effective or helpful. We show also that the results obtained on uniform grids can be significantly improved using the Richardson extrapolation and argue that it can be a good replacement for the grid stretching.

2. FORMULATION OF THE PROBLEMS AND NUMERICAL METHOD

A problem of numerical study of stability of steady axisymmetric convective flows of a Boussinesq fluid with kinematic viscosity ν^* and thermal diffusivity χ^* in an axisymmetric region $R^*_{\text{in}} \leqslant r \leqslant R^*_{\text{out}}$, $0 \leqslant z \leqslant H^*$ with respect to infinitesimally small three-dimensional perturbations is considered. The polar axis of the flow region is assumed to be parallel to the gravity force. The inner radius R^*_{in} is zero for cylindrical domains and is finite for cylindrical layers. The flow is described by the momentum, continuity and energy equations in cylindrical coordinates $(r^*,\ z^*)$. To render the equations dimensionless we use the scales $D^* = R^*_{\text{out}} - R^*_{\text{in}}$, D^{*2}/ν^*, ν^*/D^*, $\rho^*(\nu^*/D^*)^2$ for length, time, velocity and pressure, respectively. The temperature is rendered dimensionless by the relation $T = (T^* - T^*_{\text{cold}})/(T^*_{\text{hot}} - T^*_{\text{cold}})$, where T^*_{hot} and T^*_{cold} are the maximal and minimal temperatures at the boundaries of the flow region. The set of Boussinesq equations for the non-dimensional velocity $\mathbf{v} = \{v_r, v_\theta, v_z\}$, temperature T and pressure p in the domain $R_{\text{in}} \leqslant r \leqslant R_{\text{out}}$, $0 \leqslant z \leqslant A$ reads

$$\frac{\partial \mathbf{v}}{\partial t} + (\mathbf{v} \cdot \nabla)\mathbf{v} = -\nabla p + \Delta \mathbf{v} + Gr\,\theta \mathbf{e}_z \tag{1}$$

$$\frac{\partial T}{\partial t} + (\mathbf{v} \cdot \nabla)T = \frac{1}{Pr}\Delta T \tag{2}$$

$$\nabla \cdot \mathbf{v} = 0 \tag{3}$$

Here, $A = H^*/D^*$, $R_{\text{in}} = R^*_{\text{in}}/D^*$, $R_{\text{out}} = R^*_{\text{out}}/D^*$ are the aspect ratio and dimensionless inner and outer radii of the flow region, $Gr = g^*\beta^*(T^*_{\text{hot}} - T^*_{\text{cold}})D^{*3}/\nu^{*2}$ the Grashof number, $Pr = \nu^*/\chi^*$ the Prandtl number, g^* gravity acceleration, β^* the thermal expansion coefficient and $\mathbf{e}_z$ the unit

[‡] See http://www.caam.rice.edu/software/ARPACK/

[§] See http://www.enseeiht.fr/apo/MUMPS/or http://grall.ens-lyon.fr/MUMPS/

DOI: 10.1002/fld

vector in the z-direction. The boundary conditions will be specified below, separately for each problem.

The axisymmetric steady solution of (1)–(3) with the corresponding boundary conditions is calculated by a standard finite volume method as described in [1]. The non-linear terms are approximated by the conservative central differencing scheme. This approximation is chosen for the same reasons as in [1]. The finite volume grid is staggered and can be uniform or stretched. The uniform grid defined in the nodes r_i and z_j is transformed into a stretched one by

$$r_i \leftarrow R_{\text{out}}\left[\frac{r_i}{R_{\text{out}}} - a\sin\left(2\pi\frac{r_i - R_{\text{in}}}{R_{\text{out}} - R_{\text{in}}}\right)\right], \quad z_j \leftarrow A\left[\frac{z_j}{A} - b\sin\left(2\pi\frac{z_j}{A}\right)\right] \tag{4}$$

After the transformation defined by Equation (4) the grid becomes stretched near the boundaries. The density of the stretching is defined by the parameters a and b which vary between 0 and 0.12. The effect of the stretching is studied separately and is discussed for each problem considered below.

Calculation of an axisymmetric base state $\mathbf{V} = \{U(r,z), V(r,z), W(r,z)\}$, $T(r,z)$ and $P(r,z)$ proceeds in the following way. The scalar variables T and P, the azimuthal velocity component V and the divergence of velocity $\nabla \cdot \mathbf{V}$ are calculated at the nodes with integer indices $[r_i, z_j]$. The radial and axial velocity components U and W are calculated in the points $[r_{i+1/2}, z_j]$ and $[r_i, z_{j+1/2}]$, respectively, where $r_{i+1/2} = (r_i + r_{i+1})/2$ and $z_{j+1/2} = (z_j + z_{j+1})/2$. Denoting by square brackets with subscripts $[\bullet]_{i,j}$ approximation of a term in the appropriate grid node, the resulting system of steady equations reads

$$\left[U\frac{\partial U}{\partial r}\right]_{i+1/2,j} + \left[W\frac{\partial U}{\partial z}\right]_{i+1/2,j} - \left[\frac{V^2}{r}\right]_{i+1/2,j} = -\left[\frac{\partial P}{\partial r}\right]_{i+1/2,j} + \left[\frac{\partial^2 U}{\partial r^2} + \frac{1}{r}\frac{\partial U}{\partial r} - \frac{U}{r^2} + \frac{\partial^2 U}{\partial z^2}\right]_{i+1/2,j} \tag{5a}$$

$$\left[U\frac{\partial V}{\partial r}\right]_{i,j} + \left[W\frac{\partial V}{\partial z}\right]_{i,j} + \left[\frac{UV}{r}\right]_{i,j} = \left[\frac{\partial^2 V}{\partial r^2} + \frac{1}{r}\frac{\partial V}{\partial r} - \frac{V}{r^2} + \frac{\partial^2 V}{\partial z^2}\right]_{i,j} \tag{5b}$$

$$\left[U\frac{\partial W}{\partial r}\right]_{i,j+1/2} + \left[W\frac{\partial W}{\partial z}\right]_{i,j+1/2} = -\left[\frac{\partial P}{\partial z}\right]_{i,j+1/2} + \left[\frac{\partial^2 W}{\partial r^2} + \frac{\partial^2 W}{\partial z^2}\right]_{i,j+1/2} + \frac{Gr}{2}(T_{ij} + T_{i,j+1}) \tag{5c}$$

$$\left[\frac{1}{r}\frac{\partial(rU)}{\partial r}\right]_{i,j} + \left[\frac{\partial W}{\partial z}\right]_{i,j} = 0 \tag{5d}$$

$$\left[U\frac{\partial T}{\partial r}\right]_{i,j} + \left[W\frac{\partial T}{\partial z}\right]_{i,j} = \frac{1}{Pr}\left[\frac{\partial^2 T}{\partial r^2} + \frac{\partial^2 T}{\partial z^2}\right]_{i,j} \tag{5e}$$

DOI: 10.1002/fld

The indices i and j vary from 1 to N_r and N_z, respectively. To obtain the base steady axisymmetric flow, Equations (5) are solved using the Jacobian-full Newton iteration. The Jacobian matrix is evaluated analytically. The computations proceed as in [1] using the MUMPS solver at each iteration to calculate the solution of the corresponding system of linear algebraic equations.

Assuming that $\{\tilde{u}(x, y), \tilde{v}(x, y), \tilde{w}(x, y), \tilde{\theta}(x, y), \tilde{p}(x, y)\} \exp(\lambda t + \mathrm{i}m\,\theta)$ is an infinitesimally small three-dimensional perturbation characterized by the complex amplification rate λ and the azimuthal integer wavenumber m, the linear stability eigenproblem written for a calculated steady-state U, V,W, T, P reads

$$\lambda\tilde{u}_{i+1/2,j} = -\left[U\frac{\partial\tilde{u}}{\partial r} + \tilde{u}\frac{\partial U}{\partial r} + W\frac{\partial\tilde{u}}{\partial z} + \tilde{w}\frac{\partial U}{\partial z} + \frac{\mathrm{i}m}{r}V\tilde{u} - \frac{2V\tilde{v}}{r}\right]_{i+1/2,j} - \left[\frac{\partial\tilde{p}}{\partial r}\right]_{i+1/2,j} + \left[\frac{\partial^2\tilde{u}}{\partial r^2} + \frac{1}{r}\frac{\partial\tilde{u}}{\partial r} - \frac{\tilde{u}}{r^2} - \frac{m^2}{r^2}\tilde{u} + \frac{\partial^2\tilde{u}}{\partial z^2} - \frac{2\,\mathrm{i}m}{r^2}\tilde{v}\right]_{i+1/2,j} \tag{6a}$$

$$\lambda\tilde{v}_{i,j} = -\left[U\frac{\partial\tilde{v}}{\partial r} + \tilde{u}\frac{\partial V}{\partial r} + W\frac{\partial\tilde{v}}{\partial z} + \tilde{w}\frac{\partial V}{\partial z} + \frac{\mathrm{i}m}{r}V\tilde{v} + \frac{U\tilde{v} + V\tilde{u}}{r}\right]_{i,j} - \left[\frac{\mathrm{i}m}{r}\tilde{p}\right]_{i,j} + \left[\frac{\partial^2\tilde{v}}{\partial r^2} + \frac{1}{r}\frac{\partial\tilde{v}}{\partial r} - \frac{\tilde{v}}{r^2} - \frac{m^2}{r^2}\tilde{v} + \frac{\partial^2\tilde{v}}{\partial z^2} + \frac{2\,\mathrm{i}m}{r^2}\tilde{u}\right]_{i+1/2,j} \tag{6b}$$

$$\lambda\tilde{w}_{i,j+1/2} = -\left[U\frac{\partial\tilde{w}}{\partial r} + \tilde{u}\frac{\partial W}{\partial r} + W\frac{\partial\tilde{w}}{\partial z} + \tilde{w}\frac{\partial W}{\partial z} + \frac{\mathrm{i}m}{r}V\tilde{w}\right]_{i,j+1/2} - \left[\frac{\partial\tilde{p}}{\partial z}\right]_{i,j+1/2} + \left[\frac{\partial^2\tilde{w}}{\partial r^2} + \frac{1}{r}\frac{\partial\tilde{w}}{\partial r} - \frac{m^2}{r^2}\tilde{w} + \frac{\partial^2\tilde{w}}{\partial z^2}\right]_{i,j+1/2} + \frac{Gr}{2}(\tilde{\theta}_{ij} + \tilde{\theta}_{i,j+1}) \tag{6c}$$

$$0 = \left[\frac{\partial\tilde{u}}{\partial r} + \frac{\tilde{u}}{r} + \frac{\mathrm{i}m}{r}\tilde{v} + \frac{\partial\tilde{w}}{\partial z}\right] \tag{6d}$$

$$\lambda\tilde{\theta}_{i,j} = -\left[U\frac{\partial\tilde{\theta}}{\partial r} + u\frac{\partial T}{\partial r} + W\frac{\partial\tilde{\theta}}{\partial z} + w\frac{\partial T}{\partial z} + \frac{\mathrm{i}m}{r}V\tilde{\theta}\right]_{i,j} + \frac{1}{Pr}\left[\frac{\partial^2\tilde{\theta}}{\partial r^2} + \frac{1}{r}\frac{\partial\tilde{\theta}}{\partial r} - \frac{m^2}{r^2}\tilde{\theta} + \frac{\partial^2\tilde{\theta}}{\partial z^2}\right]_{i,j} \tag{6e}$$

DOI: 10.1002/fld

These equations can be written in the matrix form as

$$\lambda \mathbf{B}(\tilde{u},\ \tilde{v},\ \tilde{w},\ \tilde{p}\ \ \tilde{\theta})^{\mathrm{T}} = \mathbf{J}(\tilde{u},\ \tilde{v},\ \tilde{w},\ \tilde{p}\ \ \tilde{\theta})^{\mathrm{T}} \tag{7}$$

Here, $\mathbf{J}$ is the Jacobian matrix calculated from the r.h.s. of (6) and $\mathbf{B}$ is the diagonal matrix such that its diagonal elements corresponding to the values of $\tilde{u}$, $\tilde{v}$, $\tilde{w}$, $\tilde{\theta}$ are equal to one, while the elements corresponding to $\tilde{p}$ are zeros. The consequence of the latter is $\det \mathbf{B} = 0$. Thus, the generalized eigenproblem (7) cannot be transformed into a standard eigenproblem. To study stability of an axisymmetric steady flow state for a given set of the governing parameters, it is necessary to compute the eigenvalue λ having the largest real part for all integer azimuthal wavenumbers m. This λ is called leading eigenvalue. Apparently, $\Lambda = \max_m\{\mathrm{Real}[\lambda(m)]\} > 0$ means instability of the axisymmetric steady flow state. The value of the azimuthal wavenumber yielding the maximum of $\mathrm{Real}(\lambda)$ we call critical and denote as m_{cr}. The imaginary part of the leading eigenvalue we call critical frequency and denote as $\omega_{\mathrm{cr}} = \mathrm{Im}[\lambda(m_{\mathrm{cr}})]$. The corresponding eigenvector of (7) defines the meridional pattern of the most unstable perturbation of the base state.

Eigenproblem (7) is solved by the Arnoldi iteration in the shift-and-invert mode

$$(\mathbf{J} - \sigma \mathbf{B})^{-1}\mathbf{B}(\tilde{u},\ \tilde{v},\ \tilde{w},\ \tilde{p}\ \ \tilde{\theta})^{\mathrm{T}} = \mu(\tilde{u},\ \tilde{v},\ \tilde{w},\ \tilde{p}\ \ \tilde{\theta})^{\mathrm{T}}, \quad \mu = \frac{1}{\lambda - \sigma} \tag{8}$$

where σ is a complex shift. The ARPACK package [19] is used. To calculate the leading eigenvalue λ, it is necessary to choose the shift σ close to λ and to calculate 10–20 eigenvalues μ with the largest absolute value. The choice of σ can be an easy task if the estimate of λ is known relatively well. For many problems, like those studied in [7, 8] or one considered in Section 3.4, we fix $\mathrm{Real}(\sigma) = 0$ and vary $\mathrm{Im}(\sigma)$ until the leading eigenvalue λ is computed. Then we calculate the instability point with $\sigma = (0, \mathrm{Im}(\lambda))$ and vary $\mathrm{Im}(\sigma)$ further to ensure that there is no another eigenvalue with larger real part.

The computations proceed similar to the ones described in [1] with an addition related to the varying of the azimuthal wavenumber m. At the first stage, we calculate a steady axisymmetric flow state using the Jacobian-full exact Newton iteration. Then, the linear stability of the calculated steady flow is studied for each value of m separately. For each m, we compute the marginal value of the critical parameter, which can be Reynolds, Grashof or Marangoni number or other. The marginal value is computed by solving the equation $\max[\mathrm{Real}(\lambda)] = 0$ for a fixed m using the secant method. All other parameters during these computations are fixed. The minimum of the marginal values over all m yields the value of the critical parameter corresponding to the instability of the base flow.

As it was done in [1], we combine both Newton and Arnoldi iteration techniques with the multifrontal direct solvers for sparse matrices (we use the MUMPS solver). The efficiency of this approach is a sequence of the high level of sparseness of the Jacobian matrices of Equations (5) and (6). Using the second-order finite volume discretization scheme, these matrices are composed from banded blocks of the size $(N_r \times N_z) \times (N_r \times N_z)$, where each block have less than 15 diagonals filled by non-zero elements. Similar to two-dimensional flows in the Cartesian coordinates considered in [1], the LU-decomposition of the matrix $(\mathbf{J} - \sigma \mathbf{B})$ remains unchanged for the whole Arnoldi iteration procedure, which makes the iterations much faster than it is observed in the cases when Krylov-subspace-based iterative solvers are applied. For the Newton iteration, the efficiency of such approach is not obvious, but appears to be rather good. The characteristic times are reported in the Appendix.

DOI: 10.1002/fld

3. RESULTS

In the following, we study mainly the critical parameters corresponding to a threshold from a steady axisymmetric flow to a three-dimensional steady or oscillatory state or to an axisymmetric oscillatory flow. As in Reference [1], we argue that an accurate calculation of the critical parameters requires a good resolution of both steady-state base flow and the most unstable perturbation, that together comprise a representative benchmark exercise.

3.1. Buoyancy convection in a cylinder with parabolically heated sidewall

For the first example we consider a buoyancy convection flow in a cylinder ($R_{\text{in}} = 0$) with a parabolical temperature distribution at its sidewall

$$T(r = R_{\text{out}} = 1) = 4\left[1 - \left(\frac{z}{A}\right)^2\right] \tag{9}$$

The top and the bottom of the cylinder are kept at a constant temperature $T = 0$, so that the minimal and maximal dimensionless temperatures are 0 and 1, respectively. All the boundaries are no-slip. Details on this problem can be found in [4], where it was studied by the global Galerkin method. The results of [4] were then used in [9, 11] as a benchmark data. Here, we consider one particular case defined by $A = 2$ and $Pr = 0.03$.

The convergence of the marginal Grashof numbers and marginal frequencies for the azimuthal wavenumber m varied from 0 to 5 is shown in Table I. The calculations are carried out on the uniform finite volume grid gradually increased from 50×100 to 300×600 finite volumes by the increments of 10 in r- and 20 in z-direction. For the perturbations corresponding to $m = 3$, 4, and 5, the most unstable perturbation is steady, so that the marginal frequencies are equal to zeros and are not shown in the table. The bold rows of the table show the result of Richardson extrapolation based on two preceding grids. The last row shows the result obtained in [4] by the global Galerkin method, which is converged to within the fourth decimal digit at least. It is seen from Table I that already on a relatively coarse grid of 60×120 finite volumes it is possible to obtain two correct decimal digits of the marginal parameters. This convergence is faster than those observed for convection in rectangular cavities in [1], which is also consistent with the convergence observations of [14]. It is also clearly seen that the convergence of smaller marginal values is faster than that of the larger ones (e.g. compare convergence for $m = 2$ and $m = 0$ and 5). Note that the Richardson extrapolation can significantly improve the accuracy of results. It is clearly seen for the fine grids 290×580 and 300×600. The improvement is observed also for coarser grid for the cases where convergence of a marginal parameter is monotonic.

Table II illustrates the choice of the stretching. We pick up the critical Grashof number, which for the case considered corresponds to the azimuthal mode with $m = 2$, and focus on the grid consisting of 150×300 finite volumes. Then we vary parameters a and b in Equation (4) to choose their combination yielding the critical Grashof number closest to the result of the global Galerkin method [4]. This procedure yields $a = 0.12$ and $b = 0$ (Table II). To study the effect of this 'optimal' stretching and another stretching with $a = b = 0.12$ on the convergence of the marginal parameters, we repeat the calculations varying the grid gradually between 50×100 and 300×600 nodes. The results for $m = 2$ and 0 are shown in Figure 1(a), (b) and Figure 1(c), (d), respectively. The convergence of the marginal Grashof number (which is also critical for the

DOI: 10.1002/fld

Table I. Convergence of marginal Grashof number and marginal frequencies for natural convection in a cylinder with parabolically heated sidewall.

	$m=0$		$m=1$		$m=2$		$m=3$	$m=4$	$m=5$
$N_r=N_z/2$	Gr_m	$\omega_m/\sqrt{Gr_m}$	Gr_m	$\omega_m/\sqrt{Gr_m}$	Gr_m	$\omega_m/\sqrt{Gr_m}$	Gr_m	Gr_m	$\omega_m/\sqrt{Gr_m}$
50	520602	0.451552	331250	0.256513	96758.4	0.197462	303046	314944	789734
60	517955	0.454037	331437	0.257748	96482.2	0.197548	306931	313664	795243
70	516504	0.455559	331555	0.258482	96315.5	0.197599	309539	312928	798820
80	515663	456553	331628	0.258958	96207.1	0.197633	311351	312481	801242
90	515081	0.457242	331662	0.259285	96132.9	0.197656	312660	312181	802938
100	514697	0.457737	331723	0.259516	96079.6	0.197673	313623	311971	804169
Richardson	**513060**	**0.459847**	**331983**	**0.260501**	**95852.4**	**0.197745**	**317728**	**311076**	**809417**
110	514395	0.458105	331713	0.259693	96040.0	0.197685	314355	311818	805091
120	514210	0.458384	331686	0.259828	96009.9	0.197695	314920	311702	805795
130	514000	0.458607	331660	0.259934	95986.2	0.197702	315363	311613	806355
140	513950	0.458774	331621	0.260021	95968.1	0.197708	315722	311543	806793
150	513871	0.458913	331585	0.260093	95952.4	0.197713	316010	311486	807163
160	513759	0.459031	331551	0.260149	95940.8	0.197717	316264	311440	807442
170	513658	0.459130	331509	0.260200	95930.1	0.197720	316464	311402	806791
180	513613	0.459209	331470	0.260243	95921.9	0.197723	316633	311371	807897
190	513500	0.459283	331449	0.260286	95914.3	0.197725	316782	311344	808076
200	513554	0.459333	331395	0.260309	95908.1	0.197726	316901	311320	808217
Richardson	**514054**	**0.459796**	**330895**	**260522**	**95850.5**	**0.197735**	**318003**	**311098**	**809522**
210	513322	0.459397	331361	0.260342	95903.1	0.197728	317002	311301	808344
220	513399	0.459432	331322	0.260361	95897.1	0.197730	317102	311284	808470
230	513400	0.459460	331288	0.260384	95894.4	0.197731	317183	311269	808566
240	513399	0.459499	331255	0.260408	95890.3	0.197732	317253	311256	808637
250	513395	0.459529	331227	0.260421	95887.6	0.197733	317318	311244	808730
260	513440	0.459955	331193	0.260441	95884.8	0.197734	317373	311234	808787
270	513399	0.459573	331161	0.260449	95882.4	0.197735	317429	311225	808851
280	513416	0.459592	331128	0.260461	95880.2	0.197736	317471	311219	808895
290	513397	0.459609	331102	0.260481	95878.2	0.197736	317510	311210	808952
300	513380	0.459634	331075	0.260493	95876.2	0.197736	317546	311204	809002
Richardson	**513139**	**0.459761**	**330694**	**0.260671**	**95848.0**	**0.197736**	**318067**	**311122**	**809699**
Galerkin, 40×40 basis functions	513166	0.459876	324860	0.261444	95850.8	0.197716	318071	311110	809654

DOI: 10.1002/fld

Table II. Effect of the stretching for the critical Grashof number and critical frequency.

a	b	Gr_{cr}	$\omega_{\mathrm{cr}}/\sqrt{Gr_{\mathrm{cr}}}$
0	0	95 952.8	0.197713
0.01	0	95 944.7	0.197717
0.02	0	95 937.0	0.197721
0.05	0	95 919.3	0.197735
0.1	0	95 903.2	0.197763
0.12	0	95 901.6	0.197761
0.12	0.01	95 901.98	0.197779
0.12	0.05	95 905.1	0.197786
Result of Galerkin method		95 850.8	0.197716

Natural convection in a cylinder with parabolically heated sidewall. $A=H/R=2$, $Pr=0.03$, $N_r=N_z/2=150$.

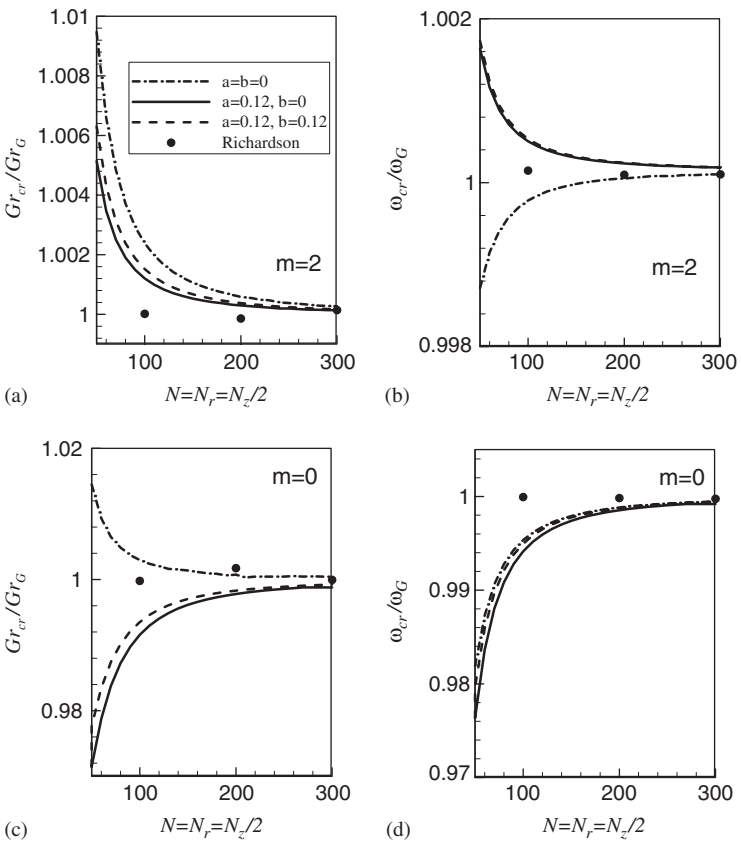

Figure 1. Convergence of the marginal Grashof number and marginal frequency for convection in a cylinder with parabolically heated sidewall. The subscript G stays for the calculation by global Galerkin method with 40×40 basis functions [4].

DOI: 10.1002/fld

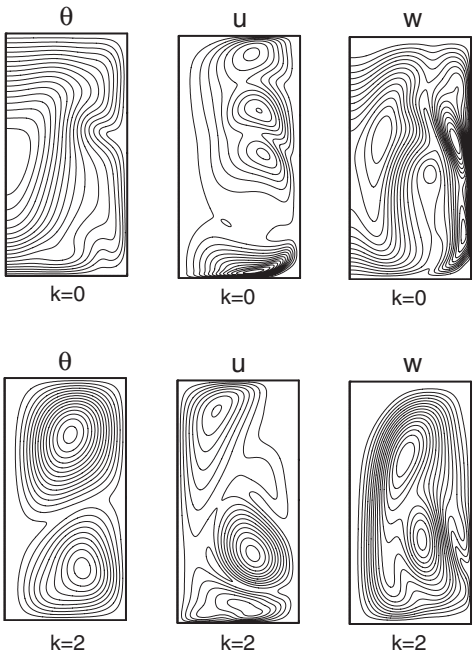

Figure 2. Modulus of the most unstable perturbations at $m = 0$ and 2 for natural convection in a cylinder with parabolically heated sidewall.

case considered) and marginal frequency for $m = 2$ is faster with the stretching. The 'optimal' stretching with $a = 0.12$ and $b = 0$ really yields a faster convergence. The results for $a = b = 0.12$ converge slower, but not significantly. When the same stretching parameters were applied for the axisymmetric mode $m = 0$, for which the marginal Grashof number is larger we did not observe any faster convergence for the stretched grids (Figure 1(c) and (d)). The reason for that is a different pattern of the marginal perturbations corresponding to two azimuthal modes. To illustrate that the modules of the complex perturbations of the temperature, radial and axial velocities are depicted in Figure 2. Note that that the 'optimal' stretching was chosen on the basis of the *a priori* known result, which is not the case for most of applied studies. The uniform grids allow for the Richardson extrapolation, which for the two examples of Figure 1 yields better accuracy than any stretching. This example shows that in cases when computations are performed on fine grids having several hundred nodes in one direction the improvement of the convergence by a stretching is not so obvious and use of fine uniform grids combined with the Richardson extrapolation can be preferable.

3.2. Thermocapillary convection in cylindrical containers

3.2.1. Liquid bridge. Computations related to thermocapillary-driven flows in containers usually are more difficult because the problem formulations can contain discontinuity points at the boundary. As a first example, we consider one of the benchmark problems defined in [2]. Flow driven

DOI: 10.1002/fld

by a thermocapillary force in a cylindrical liquid bridge ($R_{\text{in}} = 0$) located between two isothermal disks is considered. The boundary conditions for the basic flow are

$$\mathbf{v} = 0 \quad \text{at } z = 0 \text{ and } A \tag{10}$$

$$T = 0 \quad \text{at } z = 0 \quad \text{and} \quad T = 1 \text{ at } z = A \tag{11}$$

$$\frac{\partial T}{\partial r} = 0 \quad \text{at } r = R_{\text{out}} = 1 \tag{12}$$

$$U = 0, \quad \frac{\partial W}{\partial r} = -Ma\,Pr\frac{\partial T}{\partial z}, \quad \frac{\partial V}{\partial r} = -Ma\,Pr\frac{1}{r}\frac{\partial T}{\partial \theta} \quad \text{at } r = R_{\text{out}} = 1 \tag{13}$$

Here $Ma = \gamma^*(T^*_{\text{hot}} - T^*_{\text{cold}})D^*/\rho^* v^* \chi^*$ is the Marangoni number, ρ is the density and γ is the coefficient of the assumed linear dependence of the surface tension coefficient on the temperature. The boundary conditions for the perturbations are the same except Equations (11), which must be made homogeneous. It is easy to see that the derivatives $\partial W/\partial r$ and $\partial V/\partial r$ at $r = 1$ and $z = 0$ and A are zeros in Equation (10) and non-zeroes in Equation (13). Thus, the problem contains two discontinuity points, which complicate the calculations. The use of Richardson extrapolation becomes problematic in such cases because the Taylor series diverge in the vicinity of such points. Following [2, 3], we consider the case with $A = 1$, $Gr = 0$ and $Pr = 0.01$.

The exercise for the convergence study similar to one described in the previous subsection is reported in Table III and Figure 3. The axisymmetry-breaking bifurcations for $m = 1$ and 2 are steady and the corresponding zero frequencies are not reported. It is seen that two correct decimal digits of all the marginal values can be obtained using a grid with not less than 100×100 nodes. Coarser grids lead to a noticeable inaccuracy. Our result for the critical Marangoni number at $m = 2$ agrees well with results of Ermakov and Ermakova obtained on a 161×161 grid [2, 15] and with the early result of Wanshura *et al.* [3] obtained by the Chebyshev collocation method yielding much faster convergence. Other results reported in Table 10 of [2] are obtained on too coarse grids and disagree significantly with our converged result of $Ma_{\text{cr}} = 18.98$.

An interesting observation can be derived from Figure 3. The fastest convergence is observed for the azimuthal mode $m = 2$, for which the marginal Marangoni number is minimal. The next to the minimal marginal Marangoni number corresponds to $m = 1$ (Table III), however, its convergence is much slower than that of $m = 3$, in spite of the difference in the magnitudes of Ma_m.

The 'optimal' stretching was looked for as above, considering the grid 150×150 and the modes $m = 1$ and 4. It was found that the stretching values closest to those corresponding to the uniform grid 300×300 are $a = 0.12$, $b = 0.05$ for $m = 1$ and $a = 0$, $b = 0.1$ for $m = 4$. The convergence yielded by these two stretching is compared in Figure 4 with the convergence observed for the uniform grid. In this example, the stretching exhibits almost no convergence improvement compared with the uniform grid. The most striking example is seen in Figure 4(a) for $m = 1$. At the grid 150×150, the result obtained with the stretching $a = 0.12$, $b = 0.05$ is $Ma_m = 32.812$ which is very close to the value 32.8099 calculated on the 450×450 uniform grid. It is seen that the marginal number calculated using this stretching only crosses the reference value at $N = 150$, but does not converge to it. The consequent values of Ma_m calculated on the 430^2, 440^2 and 450^2 stretched grid are 32.605, 32.594 and 32.583, respectively. Here, the changes are observed in the fourth decimal digit, while the corresponding results obtained on the uniform grid (Table III) change in the fifth decimal digit, which indicates that a better convergence corresponds to the uniform grid. The stretching does not exhibit any convergence improvement for

DOI: 10.1002/fld

Table III. Convergence of marginal Marangoni number and marginal frequencies for thermocapillary convection in a cylindrical liquid bridge. Benchmark problem of [2], $Pr = 0.01$, $A = H/R = 1$.

	$m=1$	$m=2$	$m=3$		$m=4$		$m=5$	
$N_x = N_y$	Ma_m	Ma_m	Ma_m	$\omega_m Pr/Ma$	Ma_m	$\omega_m Pr/Ma$	Ma_m	ω_{cr}
50	34.2913	19.1700	73.9529	0.014494	123.6068	0.023830	101.7863	0.060859
60	33.9619	19.1114	73.4060	0.014562	121.6378	0.024159	99.5243	0.061733
70	33.7442	19.0758	73.0344	0.014604	119.9876	0.024414	98.2027	0.062292
80	33.5937	19.0525	72.7784	0.014629	118.7661	0.024595	97.3472	0.062669
90	33.4825	19.0366	72.5984	0.014647	117.9102	0.024721	96.7560	0.062934
100	33.3970	19.0251	72.4674	0.014659	117.2891	0.024812	96.3409	0.063124
Richardson	**33.0325**	**18.9761**	**71.9089**	**0.014710**	**114.6413**	**0.025200**	**94.5713**	**0.063934**
110	33.3290	19.0167	72.3698	0.014668	116.8265	0.024880	96.0356	0.063266
120	33.2736	19.0103	72.2949	0.014675	116.4751	0.024931	95.8042	0.063374
130	33.2272	19.0054	72.2364	0.014680	116.2018	0.024971	95.6253	0.063458
140	33.1879	19.0014	72.1898	0.014685	115.9852	0.025003	95.4838	0.063525
150	33.1541	18.9983	72.1518	0.014688	115.8114	0.025028	95.3696	0.063579
160	33.1245	18.9957	72.1208	0.014691	115.6682	0.025049	95.2774	0.063623
170	33.0983	18.9936	72.0950	0.014693	115.5493	0.025067	95.2008	0.063660
180	33.0749	18.9919	72.0735	0.014696	115.4498	0.025081	95.1369	0.063691
190	33.0540	18.9904	72.0550	0.014697	115.3670	0.025094	95.0831	0.063717
200	33.0350	18.9891	72.0394	0.014699	115.2958	0.025104	95.0371	0.063739
Richardson	**32.8591**	**18.9771**	**71.8950**	**0.014718**	**114.6367**	**0.025197**	**94.6113**	**0.063943**
210	33.0176	18.9881	72.0257	0.014700	115.2342	0.025114	94.9978	0.063758
220	33.0016	18.9871	72.0141	0.014702	115.1812	0.025121	94.9632	0.063775

DOI: 10.1002/fld

230	32.9869	18.9863	72.0034	0.014703	115.1338	0.025128	94.93406	0.063789
240	32.9733	18.9860	71.9948	0.014704	115.0932	0.025134	94.9081	0.063802
250	32.9607	18.9850	71.9866	0.014705	115.0566	0.025140	94.8852	0.063813
260	32.9488	18.9845	71.9797	0.014705	115.0251	0.025145	94.8647	0.063823
270	32.9378	18.9840	71.9730	0.014706	114.9971	0.025149	94.8468	0.063832
280	32.9273	18.9836	71.9671	0.014707	114.9719	0.025153	94.8305	0.063839
290	32.9175	18.9832	71.9620	0.014707	114.9481	0.025156	94.8160	0.063846
300	32.9082	18.9828	71.9583	0.014708	114.9271	0.025159	94.8032	0.063853
Richardson	**32.7756**	**18.9771**	**71.9056**	**0.014722**	**114.6278**	**0.025202**	**94.6207**	**0.063953**
310	32.8994	18.9826	71.9536	0.014708	114.9088	0.025162	94.7918	0.06386
320	32.8911	18.9823	71.9503	0.014709	114.8924	0.025165	94.7807	0.063864
330	32.8830	18.9820	71.9462	0.014709	114.8770	0.025167	94.7712	0.063868
340	32.8756	18.9819	71.9430	0.014709	114.8627	0.025169	94.7626	0.063873
350	32.8683	18.9816	71.9398	0.014710	114.8489	0.025170	94.7550	0.063877
360	32.8614	18.9814	71.9371	0.014710	114.8369	0.025173	94.7469	0.063880
370	32.8547	18.9814	71.9353	0.014710	114.8277	0.025174	94.7401	0.063884
380	32.8483	18.9811	71.9330	0.014711	114.8163	0.025176	94.7340	0.063887
390	32.8422	18.9809	71.9299	0.014711	114.8071	0.025177	94.7285	0.063888
400	32.8363	18.9809	71.9291	0.014711	114.7982	0.025179	94.7226	0.063892
Richardson	**32.7227**	**18.9809**	**71.9137**	**0.014711**	**114.6268**	**0.025218**	**94.6090**	**0.063969**
410	32.8307	18.9800	71.9268	0.014711	114.7906	0.025179	94.7176	0.063894
420	32.8252	18.9807	71.9262	0.014711	114.7832	0.025181	94.7134	0.063897
430	32.8199	18.9804	71.9238	0.014711	114.7761	0.025182	94.7089	0.063898
440	32.8150	18.9803	71.9228	0.014711	114.7695	0.025183	94.7054	0.063901
450	32.8099	18.9803	71.9208	0.014712	114.7635	0.025184	94.7017	0.063902

DOI: 10.1002/fld

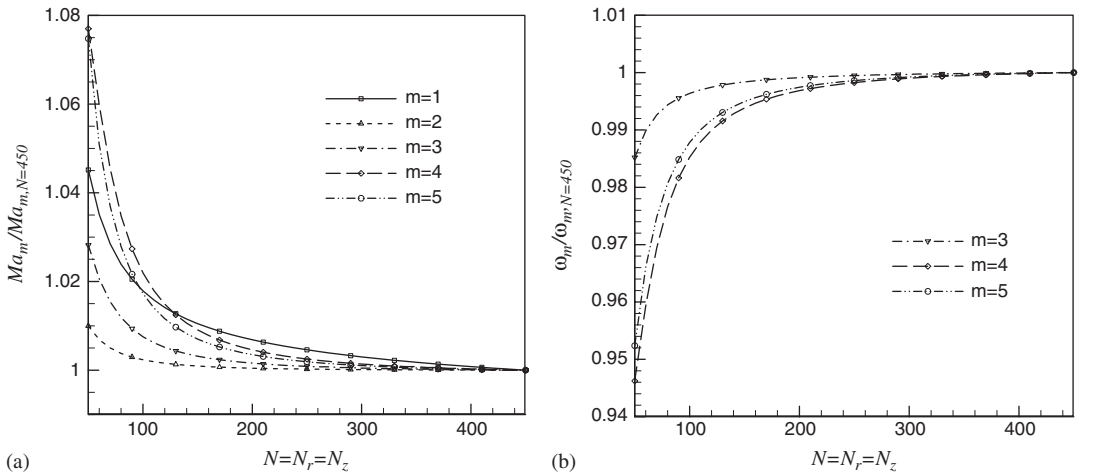

Figure 3. Convergence of the marginal Marangoni number and marginal frequency for thermocapillary convection in a cylindrical liquid bridge.

the critical mode $m=2$ (Figure 4(b)). A slight improvement in the convergence of the marginal values Ma_m is observed for $m=4$ (Figure 4(c)), which is followed by a significant convergence speedup observed for the marginal frequency (Figure 4(d)). Note, that denser stretching puts the grid points closer to the discontinuity points at the corners, which can affect the results in an undesirable way.

The bold rows of Table III contain results of the Richardson extrapolation from two preceding rows. In spite of the discontinuity points mentioned above the Richardson extrapolation can improve the result, which is most striking for coarser grids. The latter is illustrated also in Figure 4, where the Richardson extrapolation points are shown by symbols. Again, the Richardson extrapolation exhibits a significant improvement of the results calculated using the uniform grids.

3.2.2. Annular pool. Another widely studied model of axisymmetric thermocapillary convection is the flow in an annular pool (see [16–18] and references therein). The flow region is bounded by two coaxial cylinders maintained at different temperatures. The pool bottom is assumed to be no-slip and the upper surface to be flat and subjected to the thermocapillary force. Both the pool bottom and the upper surface are thermally insulated. The boundary conditions read

$$\mathbf{v}=0 \quad \text{at } R=R_{\text{in}}, \quad R=R_{\text{out}} \text{ and } z=0 \tag{14}$$

$$T=T_{\text{in}} \quad \text{at } R=R_{\text{in}} \quad \text{and} \quad T=T_{\text{out}} \text{ at } R=R_{\text{out}} \tag{15}$$

$$\frac{\partial T}{\partial z}=0 \quad \text{at } z=0 \text{ and } A \tag{16}$$

$$W=0, \quad \frac{\partial U}{\partial z}=-Ma\,Pr\frac{\partial T}{\partial r}, \quad \frac{\partial V}{\partial z}=-Ma\,Pr\frac{1}{r}\frac{\partial T}{\partial \theta} \quad \text{at } z=A \tag{17}$$

DOI: 10.1002/fld

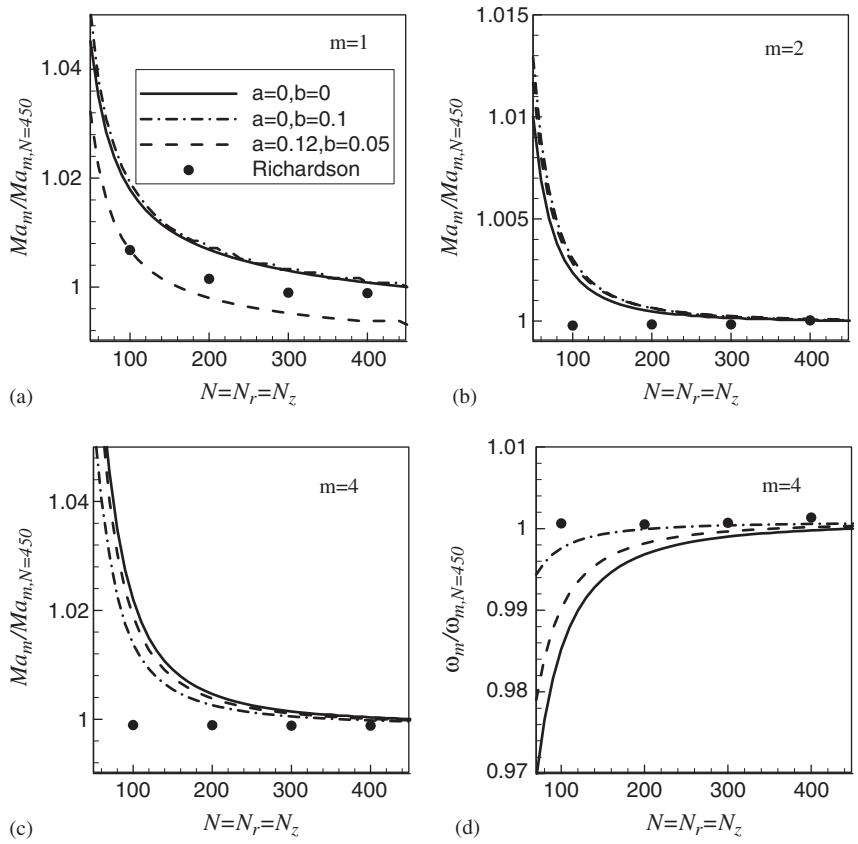

Figure 4. Effect of different stretching on the convergence of the marginal Marangoni number and marginal frequency for thermocapillary convection in a cylindrical liquid bridge.

Considering the three-dimensional instability of this flow, one concludes that this problem is more difficult for calculations than the previous one. Much finer grid is needed to obtain qualitatively correct result on the flow instability. To reach a convergence of the critical values, a further mesh refinement should be used. To illustrate how different are results obtained on different coarse grids, we refer to Table I of [16], Table II of [17], and Table I of [18].

For this study, we used parameters of [16–18] and recalculated the marginal and critical parameters on fine grids used here. The results are reported in Table IV and are compared there with the results of [16–18]. The present results are converged to within the third decimal digit at least. Comparison with the independent data shows that results are relatively close when the aspect ratio of the cavity is close to unity. The exception is the result of [17] for $A = 0.85$, where the critical Marangoni number was overestimated. When the aspect ratio decreases the critical azimuthal wavenumber grows, so that at $A = 0.15$ the azimuthal modes with $m = 10$ and 11 become critical. Clearly, such instability cannot be resolved using 60–70 grid points in the azimuthal direction, which leaves only 6–7 grid points per one azimuthal period. The marginal Marangoni numbers calculated for smaller m are closer to the results of [17], which also indicates that computations

DOI: 10.1002/fld

Table IV. Comparison of results for instability of the thermocapillary convection in an annular pool.

				Present result			Independent result			
A	$R_{\text{in}}/R_{\text{out}}$	Pr	m	Ma_m/Pr	ω_m	grid	Ma_m/Pr	ω_m	Reference	Grid $N_r \times N_\theta \times N_z$
1.111	0.1	30	2	2360	25.65	450×450	2048	2.32	[16]	$71 \times 31 \times 71$
0.85	0.5	6.7	4	1591	21.11	450×450	7651		[17]	$62 \times 63 \times 42$
0.55	0.5	6.7	3	6625	59.98	600×300	6155	57.14	[17]	$62 \times 63 \times 42$
0.3	0.5	6.7	7	2971	62.84	600×200			[17]	
0.3	0.5	6.7	2	5946	45.85	600×200	6630		[17]	$62 \times 63 \times 42$
0.15	0.5	6.7	3	6699	233.8	900×150	6719	149.2	[17]	$62 \times 63 \times 42$
0.15	0.5	6.7	10	6035	252.2	900×150			[17]	
0.15	0.5	6.7	11	6034	257.9	900×150			[17]	
1.2658	0.21	14	3	1658	24.23	450×450	1640		[18]	$30 \times 16 \times 30$

DOI: 10.1002/fld

of these authors were restricted to the modes corresponding to relatively small m. Note, that to obtain converged values of the marginal numbers, we needed more than 150 grid nodes in the shortest meridional direction.

3.3. Isothermal rotating disk–cylinder flow

For the next example, we consider an isothermal swirling flow in a stationary vertical cylinder covered by a rotating disk. All cylindrical boundaries are no-slip and the flow is defined by the cylinder aspect ratio and the Reynolds number based on the angular velocity of the disk $Re = \Omega R_{\text{out}}^2/\nu$. This problem is studied for many years (see [5, 6, 10, 12, 13] and references therein). Here, we focus on the axisymmetric and three-dimensional instabilities of this flow studied in [5, 6] by the global Galerkin method. The results of these two works were then widely used as benchmark data, e.g. in [10, 12, 13] and other studies, and were proven to be accurate to within at least the third decimal digit. Here, we use these results to examine the convergence of the finite volume method. Note, that all three velocity components of the basic axisymmetric flow of this problem are not zeros, which makes this case qualitatively different from the previous ones.

Here, we examine the convergence of the critical Reynolds number and critical frequency for different stretched grids and for three different aspect ratios of the cylinder. The results are presented in Figures 5–7. The results obtained by the global Galerkin method in [6] are denoted with the subscript 'cr, G' and are reported in the figure captions. It is seen from the figures that in this example the stretching appears to be very important for reaching a converged result. An interesting observation is that the critical parameters calculated using the uniform grid did not reach the converged values for the finest grids used, while use of some of the stretched grids (but not all of them) allowed us to converge to the critical values, which are almost identical to the results of [6]. This observation for the uniform grid is consistent with the similar ones reported in [10, 13]. Thus, the importance of a 'good' stretching can be emphasized once more.

Examination of results yielded by the Richardson extrapolation (Figures 5–7) show that for $N \geqslant 200$ they almost coincide with those yielded by the most successful stretching. This observation

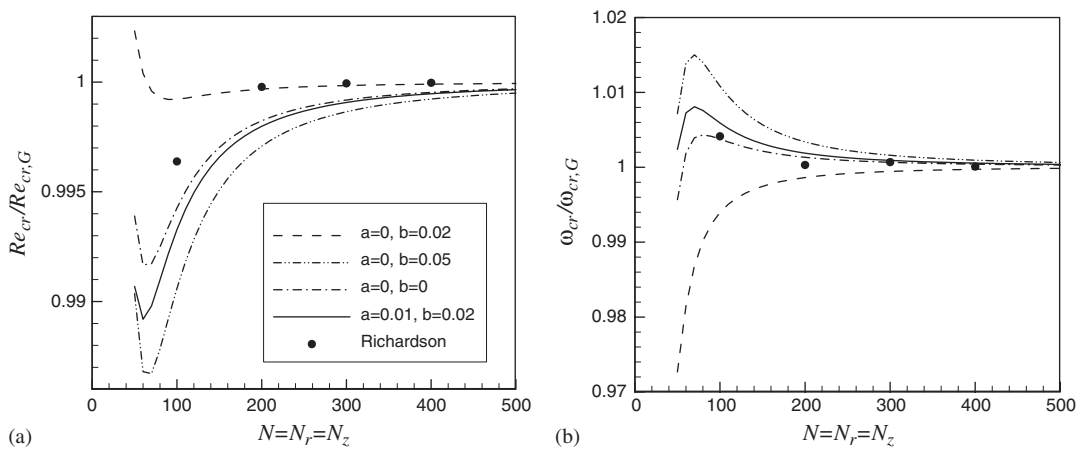

Figure 5. Effect of different stretching on the convergence of the: (a) critical Reynolds number; and (b) critical frequency for a disk–cylinder flow. $A = 1$, $m_{\text{cr}} = 2$, $Re_{\text{cr,G}} = 2471$, $\omega_{\text{cr,G}} = 0.07657$.

DOI: 10.1002/fld

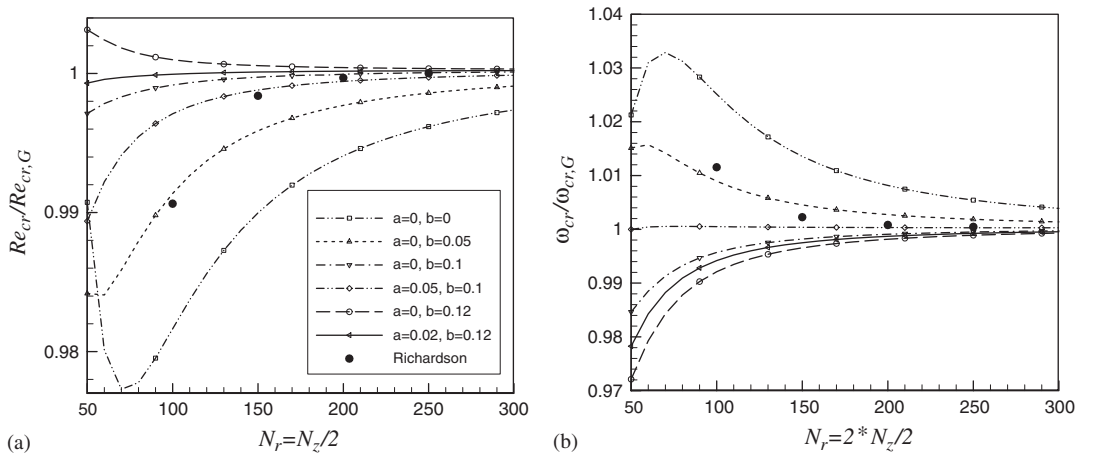

Figure 6. Effect of different stretching on the convergence of the: (a) critical Reynolds number; and (b) critical frequency for a disk–cylinder flow. $A=2.5$, $m_{\mathrm{cr}}=0$, $Re_{\mathrm{cr,G}}=2706$, $\omega_{\mathrm{cr,G}}=0.1724$.

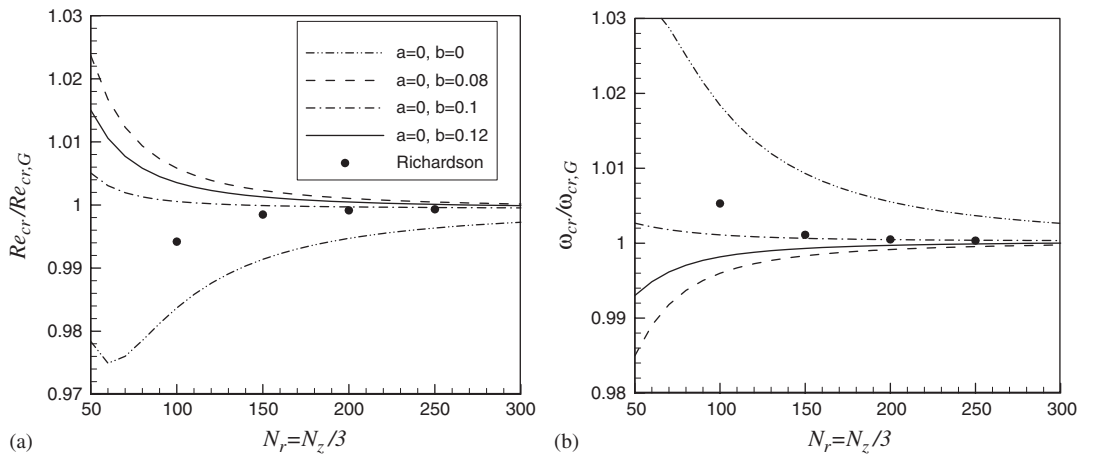

Figure 7. Effect of different stretching on the convergence of the: (a) critical Reynolds number; and (b) critical frequency for a disk–cylinder flow. $A=3.5$, $m_{\mathrm{cr}}=3$, $Re_{\mathrm{cr,G}}=2132$, $\omega_{\mathrm{cr,G}}=-0.2970$.

can be done for all six frames of Figures 5–7. A more careful observation of the results obtained on stretched grids shows that the stretching yielding the fastest convergence for the critical Reynolds number, i.e. $a=0$, $b=0.02$ for $A=1$, Figure 5(a); $a=0.02$, $b=0.12$ for $A=2.5$, Figure 6(a); and $a=0$, $b=0.1$ for $A=3.5$, Figure 7(a), does not necessarily mean the fastest convergence of the critical frequency. The frames (b) of these figures show that in all three examples the fastest convergence of the critical frequency is yielded by another stretching. At the same time, the Richardson extrapolation is always the same and yields results comparable to those yielded

DOI: 10.1002/fld

by a 'good' stretching. Therefore, this example also supports the previously made conclusion that using fine uniform grids combined with the Richardson extrapolation can be more robust than the grid stretching.

3.4. Non-isothermal rotating disk–cylinder flow

Many practically important problems relate to the flows driven by a combined action of convection and rotation. One of examples for that is the melt flow in a Czochralski crystal growth device studied by Gelfgat *et al.* [7] by a similar numerical approach. However, this flow is too complicated for the benchmark purposes. A simpler model was considered recently by Iwatsu [20]. In this model the rotating disk–cylinder flow is subjected to a non-uniform heating, so that both rotation and buoyancy force affect the flow. We follow the problem formulation of [20] and consider the cylinder with isothermal top and bottom and perfectly insulated sidewall. Assuming a convectively stable stratification, i.e. cold bottom and hot top, the temperature boundary condition reads

$$T=0 \quad \text{at } z=0, \quad T=1 \ \text{ at } z=A, \quad \frac{\partial T}{\partial r}=0 \quad \text{at } r=R_{\text{out}}=1 \tag{18}$$

Following [20] we fix the Prandtl number and the aspect ratio as $Pr=1$ and $A=1$.

The convergence studies proceed for two different cases. For the first case, we fix the Grashof number to be $Gr=10^5$ and vary the Reynolds number until the first instability sets in. This instability was found to take place at $Re=2413$ with $m_{\text{cr}}=3$ and $\omega_{\text{cr}}=-0.09017$. With the increase of the Grashof number, the stable stratification plays a more noticeable role, so that the flow stabilizes. At $Gr=10^6$ and $Re=3000$ the flow is stable. With further increase of the Grashof number the flow destabilizes again. Thus, for the second problem we fixed the Reynolds number to be $Re=3000$ and increased the Grashof number until this instability was observed at $Gr=1.0366\times 10^7$, $m_{\text{cr}}=3$ and $\omega_{\text{cr}}=-1.0241$. These two sets of critical numbers show that the dependence of Re_{cr} on Gr or Gr_{cr} on Re is not trivial. It would be interesting to map the stable flow region in the Gr–Re plain; however, this task is beyond the scope of the present study.

Since stability of such non-isothermal flow was not studied before, we report here the flow patterns (Figure 8) and the modules of the most unstable perturbations (Figures 9 and 10) for the two cases considered. At a relatively small Grashof number $Gr=10^5$ (Figure 8(a)–(c)), the patterns of meridional flow and azimuthal velocity are similar to those observed for isothermal flow (see, e.g. [5]). Modules of the most unstable perturbation (Figure 9) are also similar to those reported in [6] for the isothermal flow. At the same time, such a modest value of the Grashof number is sufficient to make the azimuthal mode $m=3$ less stable than the mode $m=2$, which is the most unstable in the isothermal case [6, 12]. Note, that in the case considered, the $m=3$ most unstable mode has $\omega_{\text{cr}}<0$, i.e. it rotates in the direction opposite to the disk rotation. The isothermal analysis of [6] predicted the same direction of rotation for this mode.

When the Grashof number increases the stable stratification suppresses the flow. Obviously, the suppression is stronger far from the rotating disk, which is observed in the flow pattern (Figure 8(d)–(f)). The meridional vortex is pushed in the upper half of the cylinder, while the flow in the lower half is almost completely suppressed. Examining the patterns of the modules of the most unstable perturbation, we notice that perturbation (Figures 9 and 10) of the meridional velocity

DOI: 10.1002/fld

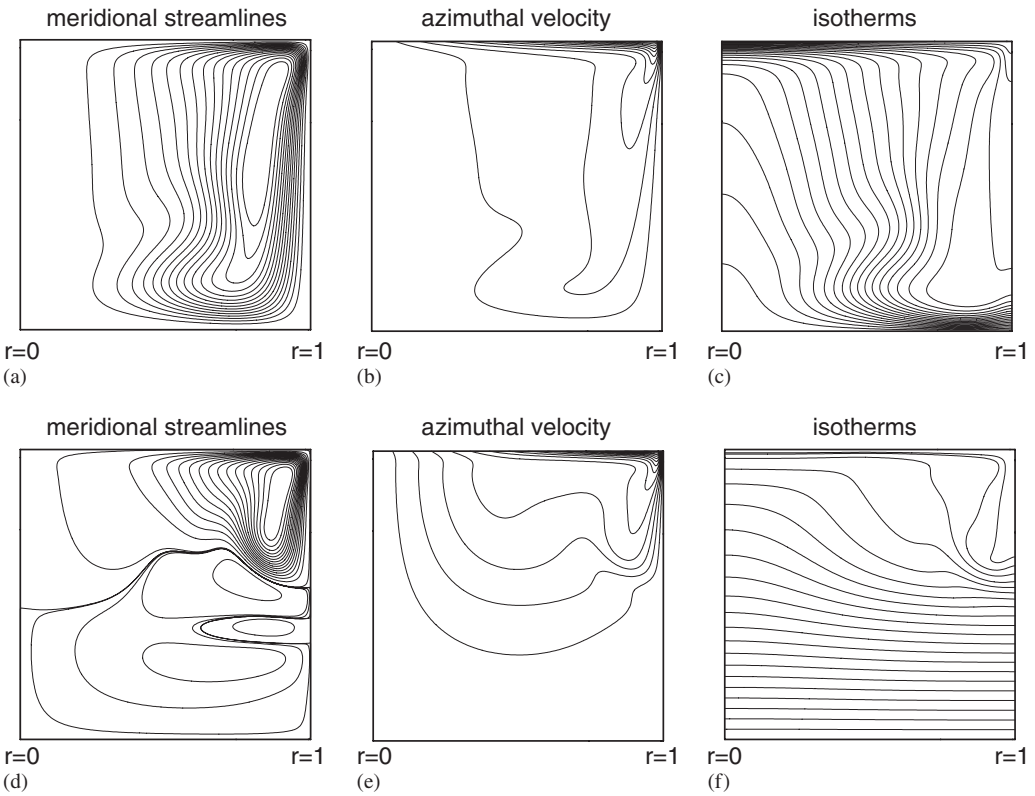

Figure 8. Flow patterns for non-isothermal rotating disk–cylinder flow; $A=1$, $Pr=1$: (a)–(c) $Gr=10^5$, $Re=2413$; and (d)–(f) $Gr=1.037\times10^7$, $Re=3000$.

components also are pushed upwards towards the rotating disk, which is most emphasized in the pattern of the radial velocity perturbation. At the same time we observe sharp maxima of the temperature and the azimuthal velocity perturbations located near the centre of the sidewall, as well as rather strong temperature perturbation in the lower half of the cylinder. Apparently, more detail studies are needed to give a satisfactory description to the instability mechanism. Here, we can only point on the qualitative difference in the perturbation patterns obtained for the two cases considered, which means that in spite of the same critical azimuthal wavenumber and the same direction of the traveling wave propagation, there exist different instability mechanisms that replace each other when the governing parameters are varied.

The convergence of the critical parameters for different grid stretching is shown in Figure 11. Based on the grid 200×200 we found that the 'optimal' stretching parameter for the case with fixed $Gr=10^5$ is $a=0$ and $b=0.04$. We repeated the calculations with this stretching and with another and denser one $a=b=0.1$, which was used for the comparison with the 'optimal' one. Among the three different sets of the stretching parameters, we observe the fastest convergence of the critical Reynolds and Grashof numbers for the 'optimal' stretching $a=0$ and $b=0.04$ (Figure 11(a) and (c)). The critical frequencies, however, converge faster when the denser stretching is used

DOI: 10.1002/fld

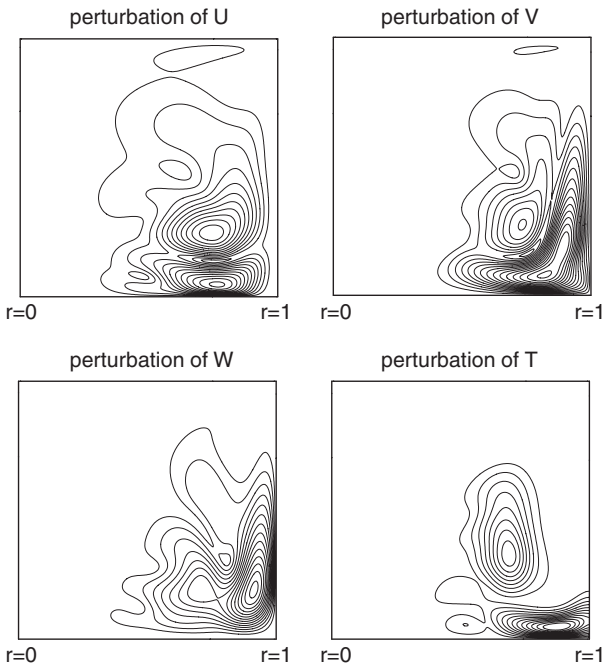

Figure 9. Modulus of three-dimensional most unstable perturbation of the non-isothermal rotating disk–cylinder flow. $A=1$, $Pr=1$, $Gr=10^5$, $Re=2413$, $m=3$, $\omega_{\mathrm{cr}}=-0.090179$.

(Figure 11(b) and (d)). Starting from the grid size 200×200 we again observe a significant improve of the results obtained on the uniform grid $a=b=0$ when the Richardson interpolation is applied. Note that the Richardson extrapolation improves only results belonging to the monotonic part of the curves shown in Figure 11. Its application to the grids 90×90 and 100×100 does not exhibit any improvement in Figure 11(a) and (b).

3.5. Rate of convergence on uniform and stretched grids

To study how numerical error vanishes with the mesh refinement, it is necessary to compare numerical results with the exact solutions. For the problems considered in Sections 3.1 and 3.3, we can use results obtained by the Galerkin method in [4, 6] and consider them as 'exact'. The relative deviation of the critical Grashof and Reynolds number is defined as $D=|(Q_{\mathrm{cr},N}-Q_{\mathrm{cr,G}})/Q_{\mathrm{cr,G}}|$, where Q stays for one of the parameters Gr or Re, the subscript cr,N corresponds to the critical value calculated on the N-nodes grid, and the subscript cr, G corresponds to the result obtained by the Galerkin method. The dependence of the deviations on the value $1/N^2$ is shown in Figure 12. Apparently, the value $1/N$ is equal to the grid size of the uniform grid and is an averaged grid size for the stretched grid.

The deviation D for the convection in a cylinder with a heated wall (Section 3.1) vanishes proportionally to N^{-2} for the uniform grid and for the stretching with $a=b=0.12$ (Figure 12(a)). When the stretching is applied in only one direction, i.e. $a=0$ and $b=0.12$ the deviation points

DOI: 10.1002/fld

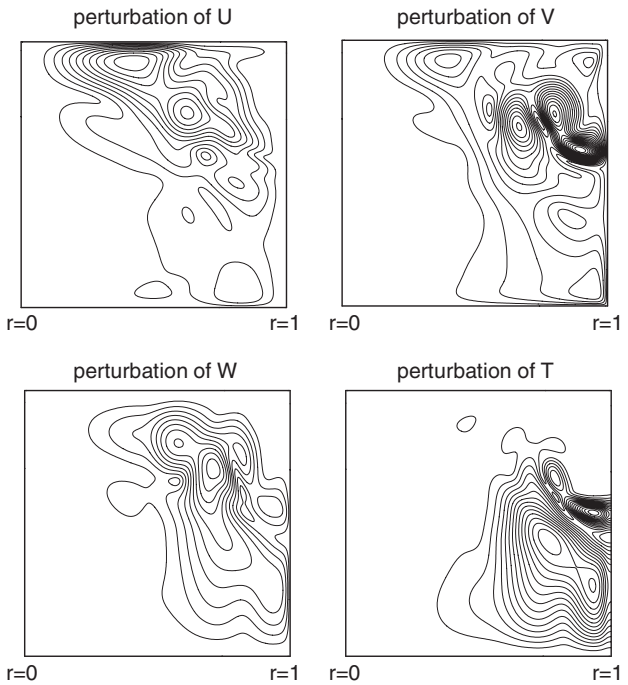

Figure 10. Modulus of three-dimensional most unstable perturbation of the non-isothermal rotating disk–cylinder flow. $A=1$, $Pr=1$, $Gr=1.037\times10^7$, $Re=3000$, $m=3$, $\omega_{cr}=-1.0242$.

depart for the straight curve; however, the tendency of the deviation decay remains proportional to N^{-2}. The problem of stability of the rotating lid–cylinder system (Section 3.3) requires a better spatial resolution. In this case, the deviation decreases proportionally to N^{-2} only starting from $N>100$ or larger (Figure 12(b)).

Since the deviation vanishes proportionally to N^{-2} also for the stretched grids, it is possible to apply the Richardson extrapolation also there. We compared the results of the Richardson extrapolation for the uniform and stretched grid and found that the results almost do not differ. Thus, for both problems related to Figure 12 the results start to differ in the fifth decimal digit. This shows that the result of the Richardson extrapolation cannot be significantly improved by a stretching.

4. CONCLUDING REMARKS

We studied the effect of grid refinement and stretching on the convergence of the critical parameters corresponding to the three-dimensional instability of axisymmetric steady flows. The whole analysis was performed using a low-order finite volume method. On the basis of above results, we can reconfirm the conclusion of [1] made for the stability problems related to convective flows in rectangular cavities. Here, we conclude once more that to obtain reliable results on flow stability

DOI: 10.1002/fld

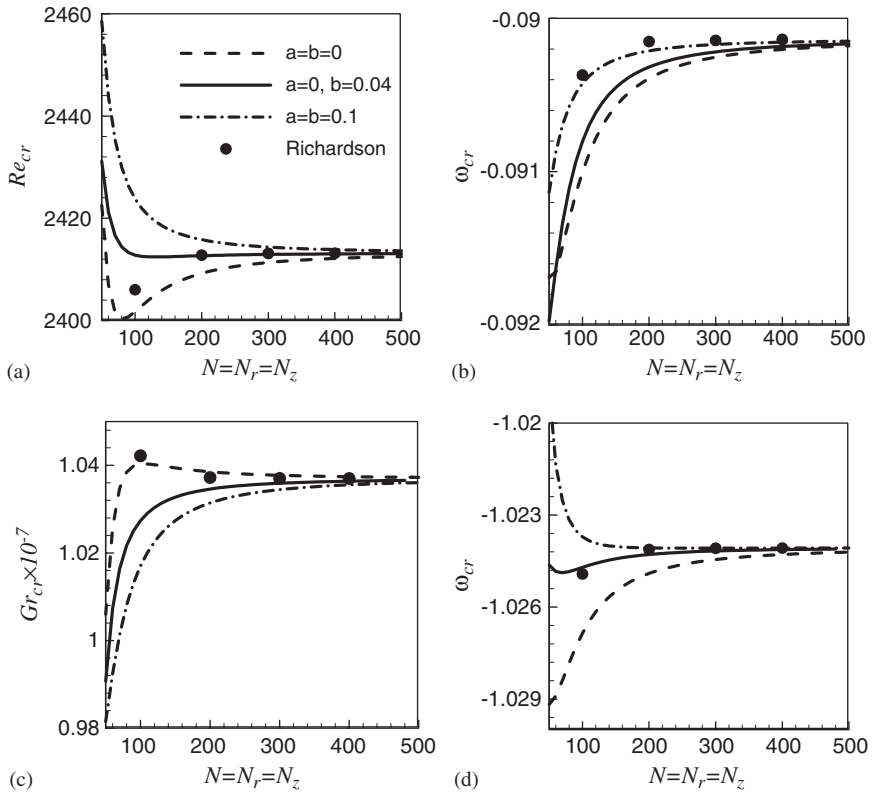

Figure 11. Effect of different stretching on the convergence of the critical parameters for patterns for non-isothermal rotating disk–cylinder flow; $A=1$, $Pr=1$: (a), (b) $Gr=10^5$, Re is varied; and (d), (e) $Re=3000$, Gr is varied.

it is necessary to use rather fine grids with at least 100 nodes in the shortest spatial direction. This finding can be confirmed also by the convergence studies of [13, 15].

The example of Section 3.1 shows that the Richardson extrapolation can significantly improve results obtained on uniform grids. It was rather unexpected to find out that for other problems considered here and having discontinuity points at the boundaries the Richardson extrapolation also significantly improves results. We showed also that the choice of a good grid stretching is not obvious and needs to be studied separately. Here, we tried to pick up 'optimal' stretching parameters on the basis of already known and sufficiently accurate result. This way did not succeed for the problem considered in Section 3.2. Apparently, this approach is not applicable to the problems where the converged result is not known *a priori*. In view of that, we conclude that a combination of fine uniform grids with the Richardson extrapolation can yield better results than an arbitrarily chosen stretching.

Finally, it is emphasized once more that the high level of sparseness of the Jacobian matrices makes calculations of their LU decompositions rather fast. The characteristic times obtained

DOI: 10.1002/fld

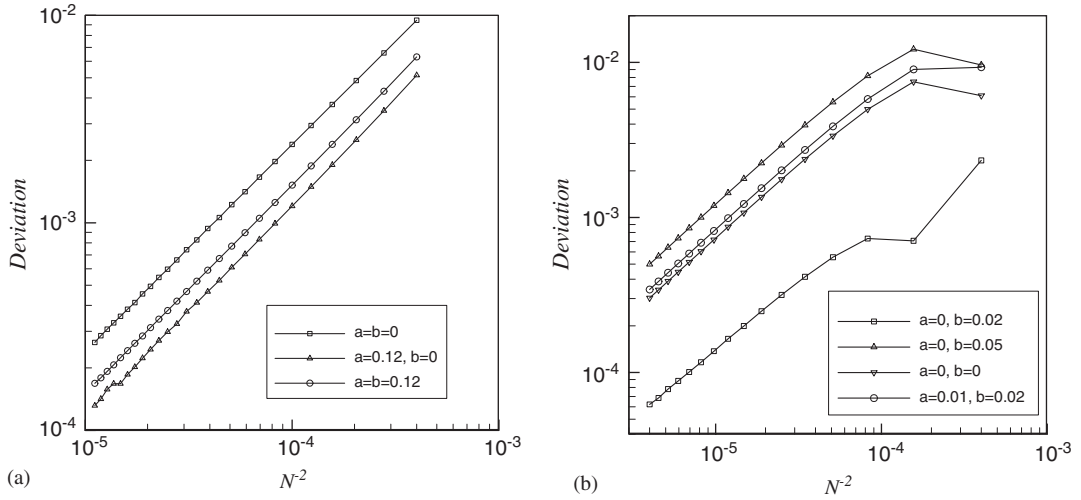

Figure 12. Deviation of the: (a) critical Grashof; and (b) Reynolds numbers obtained by the finite volume method from those calculated by the Galerkin method; (a) Problem 3.1, case of Figure 1(a); and (b) Problem 3.3, case of Figure 5(a).

using MUMPS package are given in the Appendix. The fast calculation of the LU decomposition combined with fully Jacobian exact Newton iteration for calculation of steady states and Arnoldi iteration for solution of eigenproblems allowed us to perform the detail convergence studies. It allows one also to perform the parametric stability analysis of different flows, which is planned for our future studies.

APPENDIX A

Some details on the convergence of the Newton iteration used for calculation of the steady flows and the secant method used for calculation of the marginal values of the governing parameters are given in [1]. All the estimations and conclusions made there are correct also for the present study. Here, we report the consumed central processing unit (CPU) time and memory for the problem considered in Section 3.4 (Figure A1). For this problem, the three components of velocity and the temperature must be calculated to obtain a steady-state flow, which make this problem more difficult than those considered in [1] and other sections here, for which only two velocity components were needed for a steady state. As explained above, the Jacobian matrix describing the linear stability of this flow is necessarily complex, which also makes the calculation of its eigenvalue a tougher problem. Comparison of the CPU times and memory consumed here (Figure A1) with the corresponding results of [1] shows that in the present case we need slightly longer runs and noticeably larger memory. Our estimations show that the CPU time grows as $N^{2.6}$, $N^{2.75}$, and N^2, for the real Jacobian, complex Jacobian and Arnoldi iteration, respectively, and the consumed memory grows as $N^{2.3}$ for both real and complex Jacobian matrices.

DOI: 10.1002/fld

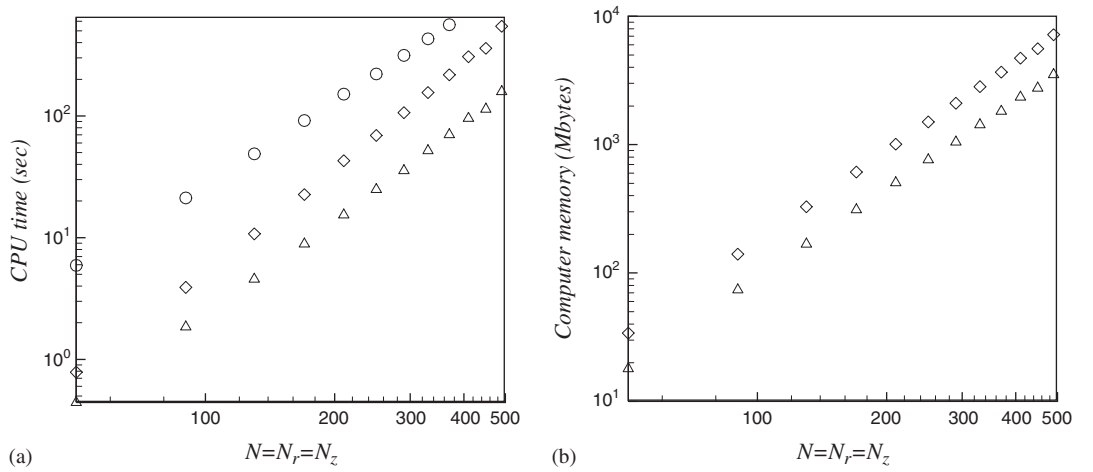

Figure A1. (a) CPU time; and (b) computer memory consumed for LU decomposition of the real Jacobian matrix needed for the Newton iteration (Δ), the complex Jacobian matrix with a complex shift needed for the sift-and-invert Arnoldi iteration (◇), and the Arnoldi eigensolvers (◯). The estimation is done for the problem considered in Section 3.4.

For other problems considered here, the estimations for the Newton iteration steady-state solver should be taken from [1], and the estimations for the eigensolvers from the above example. All the calculations reported here were carried out on the Itanium 2 personal workstation.

ACKNOWLEDGEMENTS

This study was supported by Israel Science Foundation, grant no. 156/05.

REFERENCES

1. Gelfgat AY. Stability of convective flows in cavities: solution of benchmark problems by a low-order finite volume method. *International Journal for Numerical Methods in Fluids* 2006, in press.
2. Shevtsova V. Thermal convection in liquid bridges with curved free surfaces: benchmark of numerical solution. *Journal of Crystal Growth* 2005; **280**:632–651.
3. Wanshura M, Shevtsova VM, Kuhlmann HC, Rath HJ. Convective instability mechanisms in thermocapillary liquid bridges. *Physics of Fluids* 1995; **7**:912–925.
4. Gelfgat AY, Bar-Yoseph PZ, Solan A. Axisymmetry breaking instabilities of natural convection in a vertical Bridgman growth configurations. *Journal of Crystal Growth* 2000; **220**:316–325.
5. Gelfgat AY, Bar-Yoseph PZ, Solan A. Stability of confined swirling flow with and without vortex breakdown. *Journal of Fluid Mechanics* 1996; **311**:1–36.
6. Gelfgat AY, Bar-Yoseph PZ, Solan A. Three-dimensional instability of axisymmetric flow in a rotating lid—cylinder enclosure. *Journal of Fluid Mechanics* 2001; **438**:363–377.
7. Gelfgat AY, Rubinov A, Bar-Yoseph PZ, Solan A. Numerical study of three-dimensional instabilities in a hydrodynamic model of Czochralski growth. *Journal of Crystal Growth* 2005; **275**:e7–e13.
8. Gelfgat AY, Rubinov A, Bar-Yoseph PZ, Solan A. On the three-dimensional instability of thermocapillary convection in arbitrary heating floating zones in microgravity environment. *Fluid Dynamics and Material Processing* 2005; **1**:21–31.

DOI: 10.1002/fld

9. Rubinov A, Erenburg V, Gelfgat AY, Kit E, Bar-Yoseph PZ, Solan A. Three-dimensional instabilities of natural convection in a vertical cylinder with partially heated sidewalls. *Journal of Heat Transfer* 2004; **126**:586–599.
10. Sanchez J, Marques F, Lopez JM. A continuation and bifurcation technique for Navier–Stokes flows. *Journal of Computational Physics* 2002; **180**:78–98.
11. Gemeny LE, Martin Witkowsky L, Walker JS. Buoyant instability in a laterally heated vertical cylinder. *International Journal of Heat and Mass Transfer*, to appear.
12. Marques F, Lopez J, Shen J. Mode interactions in an enclosed swirling flow: a double Hopf bifurcation between azimuthal wavenumbers 0 and 2. *Journal of Fluid Mechanics* 2002; **455**:263–281.
13. Nore C, Tuckerman LS, Daube O, Xin S. The 1 : 2 mode interaction in exactly counter-rotating von Kármán swirling flow. *Journal of Fluid Mechanics* 2003; **477**:51–88.
14. Ma DJ, Henry D, Ben Hadid H. Three-dimensional instability of natural convection in vertical cylinders partially heated from the side. *Physics of Fluids* 2005; **17**:124101.
15. Ermakov MK, Ermakova MS. Linear-stability analysis of thermocapillary convection in liquid bridges with highly deformed free surface. *Journal of Crystal Growth* 2004; **266**:160–166.
16. Sim BC, Zebib A. Effect of free surface heat loss and rotation on transition to oscillatory thermocapillary convection. *Physics of Fluids* 2002; **7**:225–231.
17. Li YR, Peng L, Akiyama Y, Imaishi N. Three-dimensional numerical simulation of thermocapillary flow of moderate Prandtl number fluid in an annular pool. *Journal of Crystal Growth* 2003; **259**:374–387.
18. Shiomi J, Amberg G. Numerical investigation of feedback control of thermocapillary instability. *Physics of Fluids* 2005; **17**:054107.
19. Lechouq RB, Sorensen DC, Yang C. *ARPACK Users' Guide*: *Solution of Large Scale Eigenvalue Problems with Implicitly Restarted Arnoldi Methods*. SIAM: Philadelphia, 1998.
20. Iwatsu R. Flow pattern and heat transfer of swirling flows in cylindrical container with rotating top and stable temperature gradient. *International Journal of Heat and Mass Transfer* 2004; **47**:2755–2767.

DOI: 10.1002/fld